Nonlinear wave surface elevation around a multi-column offshore structure

Xiudi Ren[1,2], Longbin Tao[1]*, Yibo Liang[1], Duanfeng Han[2]

[1]Department of Naval Architecture, Ocean & Marine Engineering, University of Strathclyde, Glasgow, G4 0LZ, UK

[2]School of Shipbuilding and Ocean Engineering, Harbin Engineering University, Harbin,150001, China

Abstract

Surface elevation around multiple column offshore structure is an important phenomenon crucial to air gap design of offshore platforms. This paper investigates the competing hydrodynamic phenomena, i.e., wave run-up of surface elevation rising along the column and near-trapping – the increase of surface elevation due to near-resonance among the columns. Both wave run-up and near-trapping have the characteristics of generating surface elevation peak and often impact the offshore structures with nonlinear wave loads and potentially cause slamming to platforms. With the free-surface Keulegan-Carpenter number $Kc < \mathcal{O}(1)$ and wave steepness H/L<0.14 considered, the free surface amplitude primarily depends on the diffraction pattern caused by the multiple columns and potential theory is applicable. The wave run-up and near-trapping due to wave interaction with a platform consisting of four-square columns with different corner ratios are obtained by numerical simulations. It is found that the increasing corner ratio results in a lower wave run-up under 0° incident wave, but a higher wave run-up under 45° incident wave. For near-trapping among four columns, the peak surface elevation decreases with increasing corner ratio. Two mechanisms namely superposition and near-resonance resulting the peak surface elevation are examined in detail for wave interaction with multiple columns.

Keywords: free surface elevation; multi-column structure; nonlinear waves; slamming; near-trapping

1. Introduction

With the continuing development of offshore oil and gas resources, the hydrodynamic interactions among a group of cylindrical structures attracted much attention in recent decades. There is a strong association between surface elevations and wave loads on offshore structures,

*Corresponding author: Longbin Tao longbin.tao@strath.ac.uk

especially when it comes to the nonlinear slamming loads on the deck caused by excessive vertical surface elevation. An interesting issue in designing offshore platforms is how to determine the distance between deck and water surface which is also called air gap design in order to avoid slamming which may cause serious damage to structures. The peak of surface elevation generated near column and climbing along structure is widely known as wave run-up (Kriebel, 1992). When the extreme peak surface occurs in the area enclosed by multiple columns due to large resonant motion at certain frequencies, the phenomenon is called near-trapping (Evans and Porter, 1998). In addition, free surface elevation is also associated with phenomena such as wave impacts, green water, wave deformation, rolling, spray (Shan et al., 2011). Therefore, accurate prediction of surface elevation is an essential part of the design stage of an offshore platform.

In a traditional design concept, it is used to neglect any deck slamming probability by increasing the initial air gap of platforms. The traditional air gap design method is simply to sum up the vertical response (heave motion amplitude) of the platform and wave elevation directly. This method has a great impact on the stability of the platform and increases project expenditure sharply. To avoid the over design of the air gap, several studies have been carried out to predict surface elevation which is strongly associated with air gap design (Abdussamie et al., 2017; Dong and Zhan, 2009; Fang et al., 2018; Grice et al., 2013; Low, 2010; Sweetman et al., 2001; Taylor and Sincock, 1989). The surface elevation around the offshore structures during operation and storm period was predicted well and applied in the air gap design. However, some specified environmental conditions which may lead to high surface elevation, and specific mechanisms (superposition and near-trapping) responsible for the peak surface elevation require further investigation.

Considerable research efforts have been made on the wave run-up along columns in offshore structures. Either numerical simulation or model test is performed by Raman and Venkatanarasaiah (1976), Raman et al. (1977), Chakrabarti (1978) and Kim and Yue (1989) to predict the wave run-up amplitude. However, the comparisons between numerical results and laboratory data have not generally been encouraging. Kriebel (1992) described second-order wave run-up and predicted nonlinear wave run-up distributions for 22 experimental conditions. It is found that the nonlinear diffraction theory is valid for the same relative depth and wave steepness conditions applicable to Stokes second-order plane-wave theory. Thomas and Thiagarajan (2004) investigated the wave run-up on the single fixed bottom seated cylinder in gravity waves. It was shown that the second-order harmonic component in the incident wave is important to the run-up amplitude for a single column. Xiong et al. (2015) measured the inline force for a single truncated circular cylinder in a wave tank under different submergence depths and revealed that the inline force on the single truncated cylinder is influenced by the

submergence depth, wave steepness and scattering parameters. There are also some studies about wave run-up amplitude along column with different kinds of shapes of cross-section (Grice et al., 2013; Lu et al., 2020). The circular cross-section leads to the lowest wave run-up along columns and the wave run-up amplitude along square cross-section column is the highest since the flat face.

Besides the wave run-up, the near-trapping amplitude also has a great influence on the air gap design which is directly impacted by wave run-up. The near-trapping phenomenon between columns related to geometry spaces and incident wave frequency is discussed by Linton and Evans (1990). Linear diffraction theory is applied by Evans and Porter (1997), the near-trapping amplitude is found to increase with decreasing of the space of columns. Linton and Evans (1990) and Malenica et al. (1999) revealed the relationship between incident wavelength and geometry space causing near-trapping among circular columns. Grice et al. (2013) applied the linear theory to the diffraction of regular waves by arrays of columns. Free surface amplification has been calculated using the linear model of the computer program DIFFRACT and compared between solitary columns and arrays of two and four columns. It is reported by the authors that the near-trapping phenomenon between the cylinders has been captured by the simulations based on the first-order solution. Cong et al. (2015) carried out the experiment on the diffraction of regular waves by four-cylinder structures and reported that near-trapping wave motion was observed inside the structure for a specific incident wave frequency. There are many studies on the near-trapping mode among multiple columns (Evans and Porter,1997; Dong and Zhan, 2009; Grice et al., 2013; Kagemoto et al., 2014;), and most studies are based on the circular columns due to their geometric simplicity (Evans and Porter,1997; Dong and Zhan, 2009; Kagemoto et al., 2014;). Few works are carried out on the near-trapping among the square columns or rounded-corner square columns.

There are many factors influencing the wave surface elevation around offshore structures like fixity and the existence of pontons. By comparing the experimental results of platforms with and without pontoons linked to the columns, the surface elevation is found to be slightly smaller in the absence of the pontoons (Niedzwecki and Huston,1992). Simos et al. (2008) performed small-scale model tests of the air gap response of a floating semi-submersible. It is revealed that the first-order numerical solution seriously underestimates the wave run-up. Shan et al. (2011) investigated the surface elevation around different columns of a semi-submersible. The model tests were conducted for both floating and fixed models and it was found that the wave run-up for the floating semi-submersible is significantly smaller than that for the structure being fixed. In addition, the results indicated that the wave shape close to the columns shows higher harmonic characteristics due to the interaction between waves and columns of the semi-submersible platform.

Considerable effort has been made to theoretically predict the surface elevation or wave run-up using the computational fluid dynamics (CFD) method. Wang and You (2009) used Fluent solver based on the Navier-Stokes (N-S) equations to simulate the interaction of viscous wave fields with a fixed semi-submersible platform. It is revealed that the viscous effect reduces the wave run-up on the columns of the platform. Dong and Zhan (2009) obtained wave elevation and run-up along a fixed circular column in shallow water based on the N-S equations applying the volume of fluid (VOF) method for the free surface. Good agreement was observed between numerical simulations and experimental measurements. Chen et al. (2014) generated regular waves and focused waves by using OpenFOAM and carried on investigating wave run-up and wave load on a single column wind turbine under the regular wave and focused wave. Their results captured the higher order harmonic components of wave run-up and wave load showed agreement with experimental measurement. Lin et al. (2017) developed a CFD model for simulating different types of wind turbines at sea. The results showed that the wave run-up and wave load of these models under small wave steepness are even higher than that for larger wave steepness at some incident wave frequency, and the authors attributed that to the near-trapping phenomenon.

It is acknowledged that the CFD method can be accurate in capturing the interaction between water and air in wave breaking or wave run-up. However, for large structures with the free-surface Keulegan-Carpenter number, $Kc=A/a<O(1)$ ("A" and "a" being the wave amplitude and cylinder radius, respectively), the potential theory is applicable. For A/a less than of order unity, the flow around the cylinder will not separate and the fluid domain can be described by potential theory (Thomas and Thiagarajan, 2004).

Potential flow theory based numerical model provides a more effective way to solve the wave-structure interactions often involving the prediction of nonlinear surface elevation and wave loads on offshore structures. Wang and Wu (2010) investigated an array of cylinders in a numerical wave tank. Free surface elevation and hydrodynamic force were obtained for both bottom-mounted and truncated cylinders. Sweetman et al. (2001) used the commercial program WAMIT in which the second-order nonlinearities were included to predict the air gap response of a semi-submersible. Kristiansen et al. (2004) conducted the mesh sensitivity study of columns and free surface for the second-order nonlinear wave run-up.

Since the rounded-corner square column is one of the most common types used for construction of offshore structures, and the impact of the ratio of the corner radius for rounded-corner square columns has not been properly investigated. In the present work, the potential theory-based program will be used to solve the diffraction potential and surface elevation around the multiple columns where the incident wave is perturbed to the second-order. A number of physical

parameters important to the surface elevation are examined in detail including the cross-section of the columns, ratio of the rounded corner of square columns and incident wave direction crossing multiple columns. It is noted that the highest surface may not only occur around the columns due to the interaction of multiple columns, thus the surface elevation analyzed here is not only along the columns but also the entire area under the deck of the platform. A fully second-order solution of the surface elevation is obtained for the wave diffraction problem.

In the main part of this paper, numerical simulations of the first- and second-order diffraction are conducted by using an industry standard numerical tool WAMIT (Lee, 1995). The model setup and mesh convergence study are presented in Section 3. The detailed results and discussions on the surface elevation for different types of columns and platforms are presented in Section 4.

2. Methodology

In this study, the numerical simulation is based on the potential flow theory. Considering the fluid is ideal, free of separation or lifting effects, and is governed by the Laplace equation. The wave is assumed as the small amplitude wave for the perturbation method being applicable. To obtain the nonlinear solutions for both wave surface elevation and wave load, the velocity potential has been perturbed to second-order in diffraction analysis (Kim and Yue, 1989, 1990).

$$\phi = \varepsilon\phi^{(1)} + \varepsilon^2\phi^{(2)} + \ldots \tag{1}$$

$$\phi^{(1)}(x,y,z,t) = \mathrm{Re}\left\{\phi^{(1)}(x,y,z)e^{-i\omega t}\right\} \tag{2}$$

$$\phi^{(2)}(x,y,z,t) = \mathrm{Re}\left\{\phi^{(2)}(x,y,z)e^{-i2\omega t}\right\} + \overline{\phi}^{(2)}(x,y,z) \tag{3}$$

where ϕ is the total velocity potential, $\phi^{(1)}(x,y,z,t)$ is the first-order velocity potential and $\phi^{(2)}(x,y,z,t)$ is the second-order velocity potential. $\phi^{(1)}(x,y,z)$ and $\phi^{(2)}(x,y,z)$ are the time independent velocity potentials and $\overline{\phi}^{(2)}$ is the mean level of the velocity potential.

The first-order and the second-order velocity potential satisfy Laplace's equation and the boundary conditions in diffraction analysis. For the first-order,

$$\nabla^2\phi_D^{(1)} = 0 \quad z > 0 \tag{4a}$$

$$(-\omega^2 + g\frac{\partial}{\partial z})\phi_D^{(1)} = 0 \quad z = 0\left(S_F\right) \tag{4b}$$

$$\frac{\partial \phi_D^{(1)}}{\partial z} = 0 \quad z = -h \tag{4c}$$

$$\frac{\partial \phi_D^{(1)}}{\partial n} = -\frac{\partial \phi_I^{(1)}}{\partial n} \tag{4d}$$

$$\lim_{k\rho\to} \rho^{1/2}(\frac{\partial}{\partial \rho} - ik)\phi_D^{(1)} = 0 \tag{4e}$$

and for the second-order diffraction analysis,

$$\nabla^2 \phi_D^{(2)} = 0 \quad z > 0 \tag{5a}$$

$$(-4\omega^2 + g\frac{\partial}{\partial z})\phi_D^{(2)} = q \quad z = 0\left(S_F\right) \tag{5b}$$

$$\frac{\partial \phi_D^{(2)}}{\partial z} = 0 \quad z = -h \tag{5c}$$

$$\frac{\partial \phi_D^{(2)}}{\partial n} = -\frac{\partial \phi_I^{(2)}}{\partial n} \tag{5d}$$

$$\lim_{k\rho\to} \rho^{1/2}(\frac{\partial}{\partial \rho} - ik)\phi_D^{(2)} = 0 \tag{5e}$$

where ϕ_D is the diffraction wave potential, ω is the incident wave frequency, and k is the incident wave number. The right-hand side term "q" in (5b) is the non-homogeneous term that represents the free surface condition and shows the quadratic production of the first-order potential.

Free surface elevation

The free surface elevation is decomposed into four parts: the first-order component, the time-independent component, the second-order quadratic component, and the second-order potential component. Thus, the elevation is written as:

$$\xi^{(1)} = -\frac{1}{g}\frac{\partial \phi^{(1)}}{\partial t} \tag{6}$$

$$\xi^{(2)} = -\frac{1}{g}(\frac{\partial \phi^{(2)}}{\partial t} + \frac{1}{2}(\nabla \phi^{(1)})^2 - \frac{1}{g}\frac{\partial \phi^{(1)}}{\partial t}\frac{\partial^2 \phi^{(1)}}{\partial z \partial t}) \tag{7}$$

where $\phi^{(1)}$ and $\phi^{(2)}$ is the first-order and the second-order wave potential, respectively, z is the z-axis direction, and t is time.

187 The total surface elevation up to the second-order is given as

188 $$\xi = \xi^{(1)} + \xi^{(2)} \tag{8}$$

189 where, the ξ , $\xi^{(1)}$ and $\xi^{(2)}$ is the total surface elevation, the first-order elevation and the
190 second-order elevation respectively. g is the gravitational acceleration. In this study, the
191 surface run-up will be considered under the combination of the incident wave and diffraction
192 wave. Therefore, the velocity potential in (1) can be written as (Wang and Wu, 2007),

193 $$\phi^{(1)} = \phi_I^{(1)} + \phi_D^{(1)} \tag{9}$$

194 $$\phi^{(2)} = \phi_I^{(2)} + \phi_D^{(2)} \tag{10}$$

195 The boundary value problem (BVP) governing the wave-structure interaction has been
196 decomposed into the first-order and second-order problems, and the diffracted wave velocity
197 potential of the first- and second-order is solved by the BVPs respectively.

198 *Model configurations*

199 Regular wave is considered as incident wave with the direction of 0° and 45° respectively (see
200 Fig 1). For nonlinear analysis, the incident wave is perturbed to the second-order, both the
201 quadratic first-order potential term and the second-order potential term are taken into
202 consideration in the calculation of surface elevation. Sum- and difference-frequencies
203 contribution to the surface elevation and inline force are also calculated. All simulations are
204 carried out by the hydrodynamic program WAMIT through commercial software SESAM.

205

206 (a)

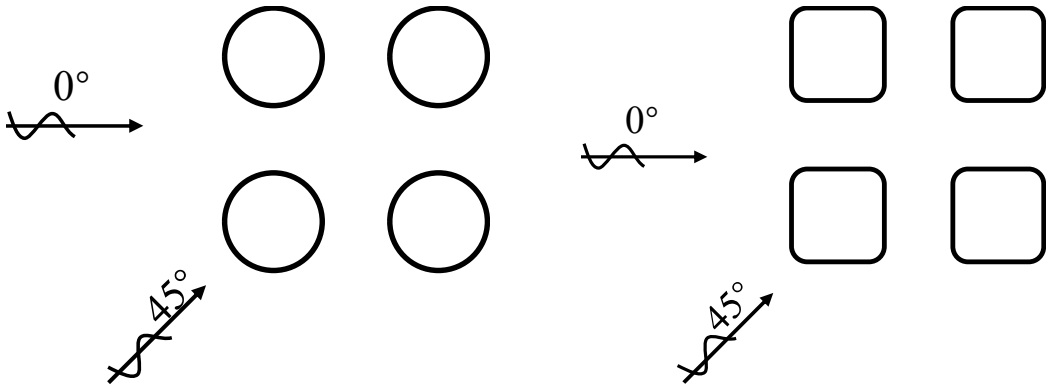

(b)

Fig 1 (a): Configuration of single column; (b): 4 columns with 0°and 45°incident wave.

The principal dimensions of cylinders analysed in the study are given in Table 1 and the wave conditions are shown in Table 2. The arrangements of the columns with different cross-sections are shown in Fig 1.

Table 1. The dimension of cylinders

Cylinder type	**Diameter**	**Leg spacing**	**Corner-ratio**
Circular column	*D*	Single, Four-columns 2*D*	---
Sharp corner column	*D*	Single, Four-columns 2*D*	1/2
Rounded corner-square column	*D*	Single, Four-columns *2D*	1/3,1/4 and 1/6

Table 2 Wave conditions in the numerical simulation

Wave Conditions	**Scattering parameters *ka***	**Wave steepness *H/L***
WC1	0.1-1.0	0.04
WC2	0.1-1.0	0.05
WC3	0.1-1.0	0.064

3. Mesh convergence

A mesh sensitivity study has been carried out with different levels of mesh resolution for the simulation. The non-dimensional parameters of structure and incident wave in the sensitivity study have been kept the same. The scattering parameter is set to ka = 1.0, wave steepness is set to H/L=0.064 (H is wave height, and L denotes wavelength) and leg space is *2D* for 4 columns configuration, which is the strongest nonlinear condition in all the following simulations. Both surface elevation and the inline force have been calculated in the mesh sensitivity study. The leg space represents the distance between the centres of the columns for

the multiple cylinder groups. The discretisation is carried out on both the column surface and the free surface as required by the second-order analysis. The mesh options have been listed in Table 3 and Table 4 for the single cylinder and the 4 cylinder cases respectively.

Table 3 Mesh options for the single cylinder and the second-order free surface

No.	Column surface mesh	No.	Free surface mesh
C1	400	F1	3000
C2	1500	F2	4000
C3	2400	F3	4800
C4	4800	F4	7650
C5	9600	F5	9000

In Table 3, there are 5 options for both column surface mesh and the free surface mesh. To avoid the influence between the two kinds of mesh, when investigating the mesh for the column, the mesh for the free surface has been set constant.

Table 4 Mesh options for the 4 columns configuration and the second-order free surface mesh

No.	Column surface mesh (1/4)	No.	Free surface mesh (1/4)
C1	400	F1	2700
C2	1500	F2	3920
C3	2400	F3	5070
C4	4800	F4	7800
C5	9600	F5	9250

Similar kinds of mesh for 4 cylinders configuration are listed in Table 4. Since the symmetrical configuration, only one-quarter of the mesh number is presented in Table 4. The method of convergence study is the same as the single cylinder case. The surface elevation and non-dimensional inline force calculated using different meshes are plotted in Fig 2 and Fig 3, and a clear trend of convergence for both physical quantities are evident. With the consideration of the two kinds of mesh and the computational time, the mesh of C4F4 (4800x7650) and the C4F5 (4800x9250) are selected for the simulation of the single cylinder case and the 4 cylinders case respectively.

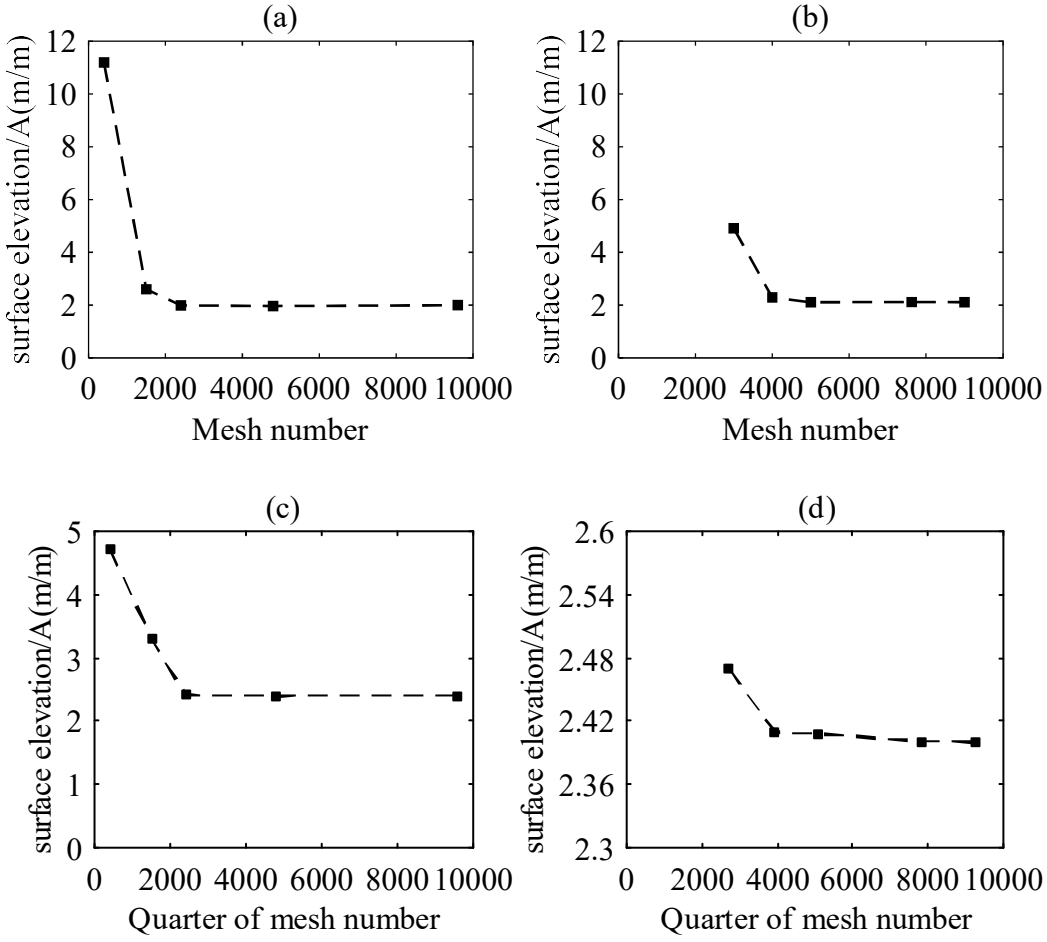

Fig 2 Surface elevation. (a): Column surface mesh convergence for the single fixed column with free surface mesh F5, (b): Free surface mesh convergence for the single fixed column with column surface mesh C5. (c): Column surface mesh convergence for the 4 fixed columns with free surface mesh F5 (d): Free surface mesh convergence for the 4 fixed columns with column surface mesh C5.

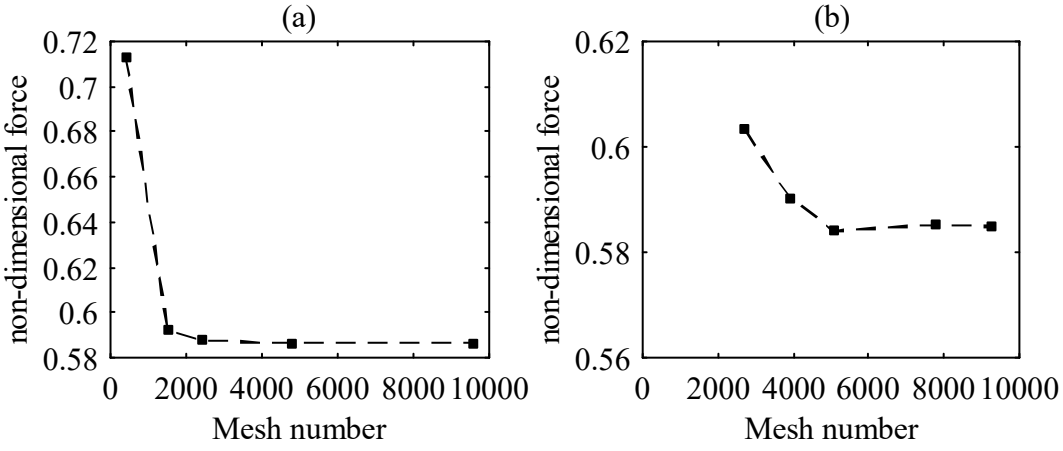

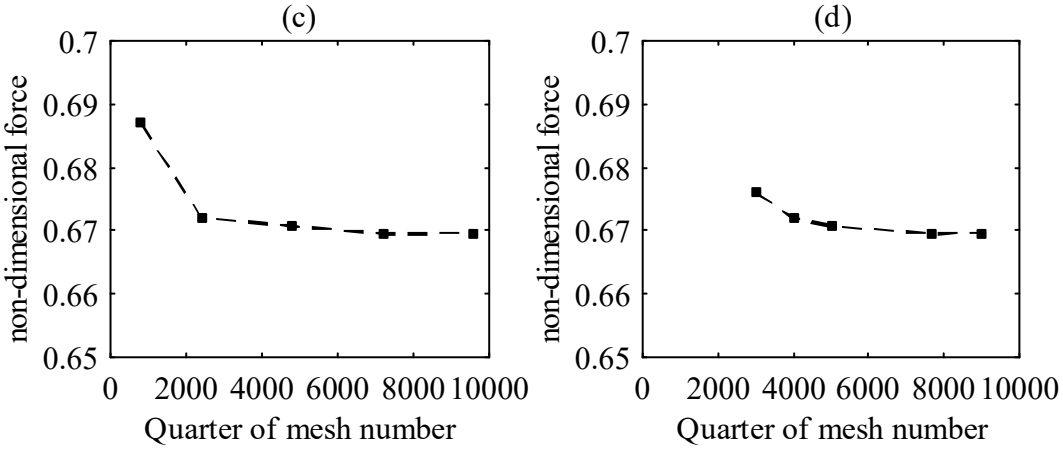

Fig 3 Inline wave force. (a): Column surface mesh convergence for the single fixed column with free surface mesh F5, (b): Free surface mesh convergence for the single fixed column with column surface mesh C5. (c): Column surface mesh convergence for the 4 fixed columns with free surface mesh F5 (d): Free surface mesh convergence for the 4 fixed columns with cylinder surface mesh C5.

The inline force shown in Fig is non-dimensionalised by $\rho gHDd[\tanh(kd)/kd]$, where 'H' is the incident wave height, 'D' is the diameter of the cylinders, 'd' is the water depth, and 'k' is the wave number. As can be seen in Fig and 3, while simulations using the different mesh on the column approach to the converged results quickly for finer mesh, the requirement for the free surface mesh is considerably higher for the second-order free surface modelling.

4 Results and discussion

4.1 Effect of the cross-sectional shape of single column on wave run-up

There are different kinds of column shapes of cross-section often be applied in the offshore structure design. Considerable research effort has been made about the impact of the shape of cross-section on wave run-up amplitude along column (Grice et al., 2013; Lu et al., 2020). However, there are very few studies focusing on the impact of the rounded corner ratio of squared column on the run-up amplitude along the vertical column. There are three kinds of cross-sectional shapes applied on the column in the present work, circular, rounded corner square (with three different ratios, 1/6, 1/4 and 1/3) and the sharp corner square to investigate the relationship between the surface elevation and the ratio of column corner. Each column shape has the same cross-sectional diameter to keep the same diffraction parameters of each column shape.

The validation of wave run-up amplitude around the single column is presented firstly in Fig 4, and the run-up amplitude of the present numerical results agree well with the experimental measurements of Thomas and Thiagarajan (Thomas and Thiagarajan, 2004) for both scattering parameters calculated, ka=0.417 and ka=0.698 respectively.

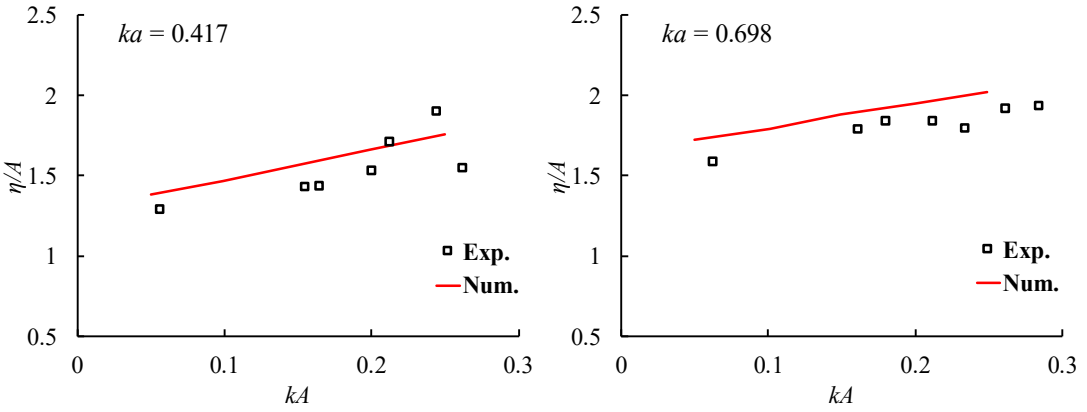

Fig 4 Wave run-up on a single column: Numerical results vs. Experimental measurements. (η is the total surface elevation; A is the incident wave amplitude)

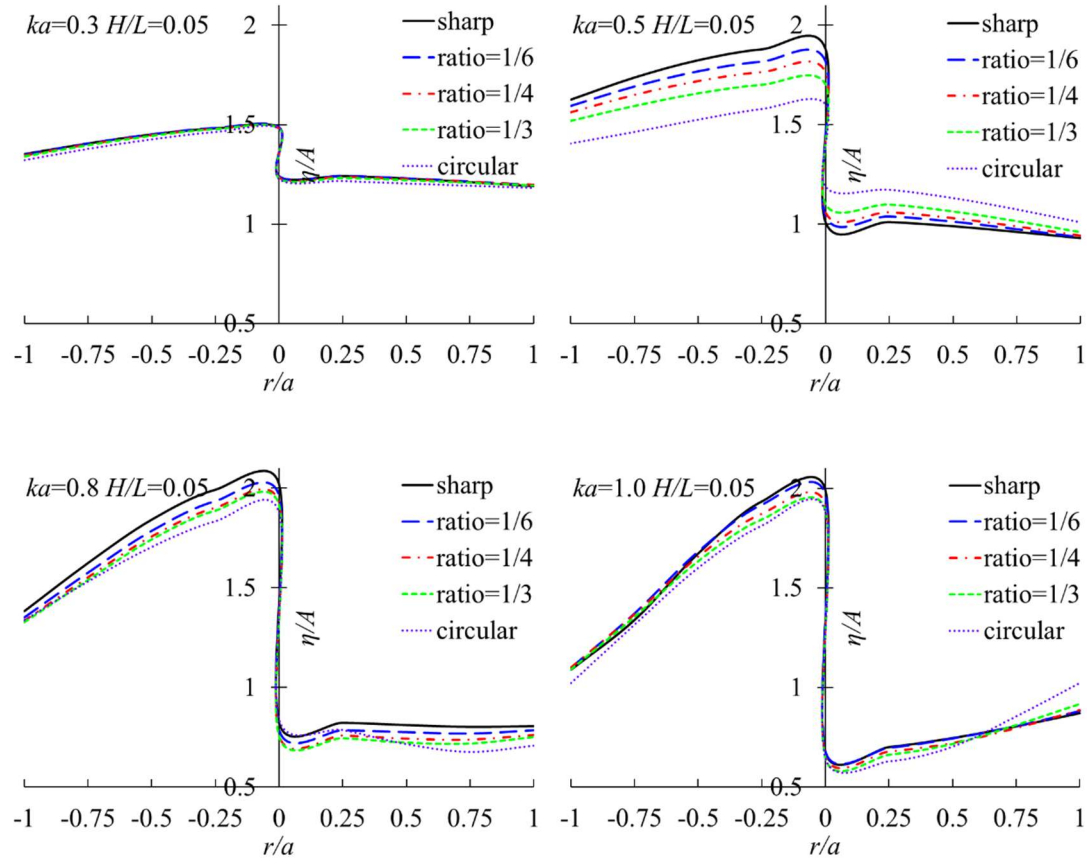

Fig. 5 The wave profile near the column under 0° incident wave with different corner ratio columns (η is the total surface elevation; A is the incident wave amplitude)

As one of the primary parameters crucial to the nonlinear wave interaction with offshore structures, scatter parameter can have a significant impact on the nonlinear wave run-up and subsequent wave loads on offshore structures. The wave profile near single column in the incident wave direction at different scatter parameters ka=0.3, 0.5, 0.8 and 1.0 are calculated and shown in Fig 5 with the incident wave from 0° with the wave steepness H/L=0.05 (H is the wave height and L is the wavelength). The wave profile before reaching the column is shown on the negative of the X-axis and the profile behind the column is shown on the positive. The sharp corner square column and the circular column can be treated as special cases with ratio=0 and 1/2 respectively. There is a very slight difference in the wave run-up caused by columns of different corner ratios when ka=0.3 because the wavelength is much longer than the diameter of the column. With higher scatter parameters like ka=0.5, 0.8, and 1.0, there is a more obvious impact of corner ratio on the wave run-up amplitude because of the shorter wavelength comparing to the column diameter. The higher corner ratio of the column evidently leads to lower wave run-up amplitude both upstream and downstream of the column when ka=0.5, 0.8 and 1.0. However, there is an exception of the downstream for ka=0.5 where a reverse trend can be observed for the wave run-up caused by different corner ratios of column indicating that the impact of the corner ratio on wave run-up is not uniform with the crossing scatter parameter.

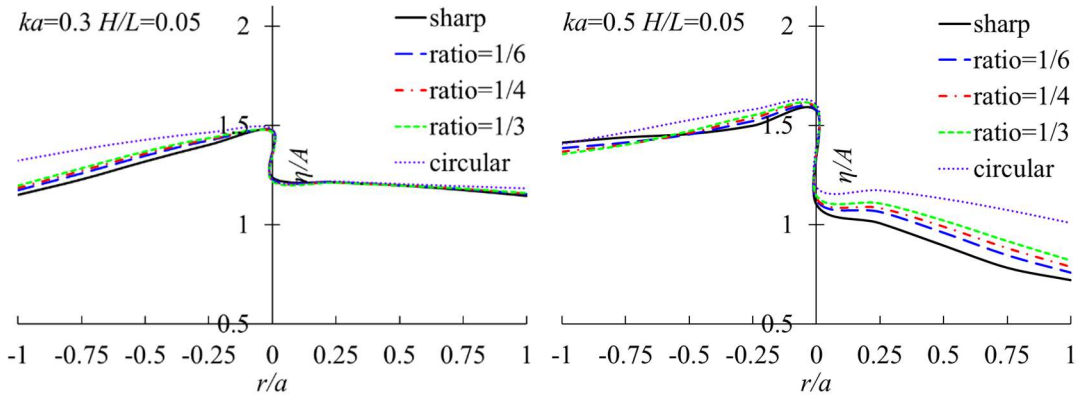

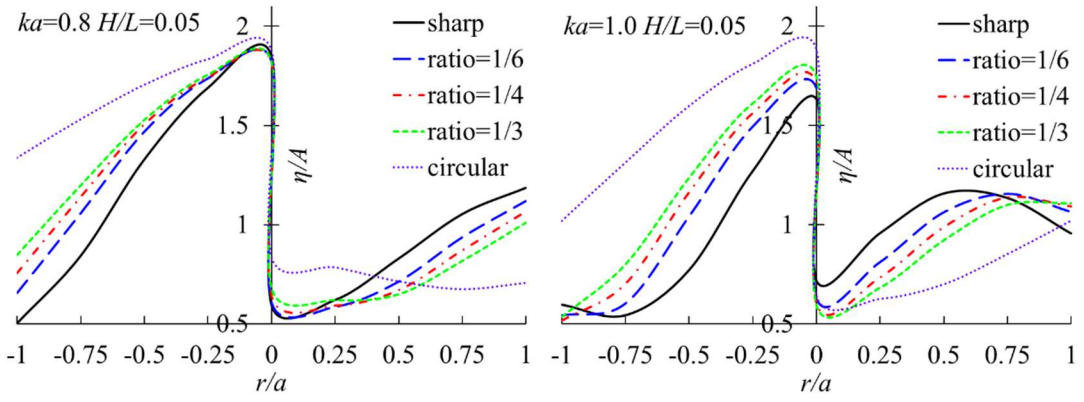

Fig. 6 The wave profile near the column under 45° incident wave with different corner ratio columns (η is the total surface elevation; A is the incident wave amplitude)

The wave profile near columns is shown in Fig. 6 for the 45° incident wave. A general trend can observe that in all cases, a high corner ratio tends to lead to higher wave run-up upstream while result in lower wave run-up downstream noting that very little impact on wave run-up for ka=0.3 where the diameter of the column is very small comparing to the incident wavelength. For all cases presented with different scatter parameters, the wave run-up is more sensitive to corner ratio with higher scatter parameter. At low ka (0.3 and 0.5), the surface profile appears to increase approaching the column and decrease downstream modestly, while for high ka (0.8 and 1.0), the free surface shows a sharp increase approaching the column followed by a clear increasing trend leaving the column downstream. Fig. 6 demonstrates that the corner ratio has a significant impact on nonlinear wave run-up especially for high scatter parameter conditions and thus should be considered in air gap design for offshore structures.

4.2 Multiple columns

4.2.1 Near-trapping phenomenon in four columns structure

Four-columns structures are widely used in offshore engineering. The interaction between columns and waves can lead to complex diffraction patterns around multiple columns. The near-trapping phenomenon is a near-resonant free surface response that is excited by waves of the appropriate frequency interacting with structures (Linton and Evans,1990). There are many studies on the near-trapping mode among multiple columns (Evans and Porter,1997; Dong and Zhan, 2009; Grice et al., 2013; Kagemoto et al., 2014;), and most studies are based on the circular columns due to their geometric simplicity (Evans and Porter,1997; Dong and Zhan, 2009; Kagemoto et al., 2014;). There are few works on the near-trapping among the square columns or rounded-corner square columns. Comprehensive numerical simulation has been conducted to further examine the phenomenon especially the detailed first- and second-order contributions on multiple column structures with variety of cross-sectional shapes, as well as under different incident wave directions. The numerical model with free surface mesh is firstly validated using the free surface elevation before the downstream column against experimental measurements of Giorgio et al. (2004), as shown in Fig 7.

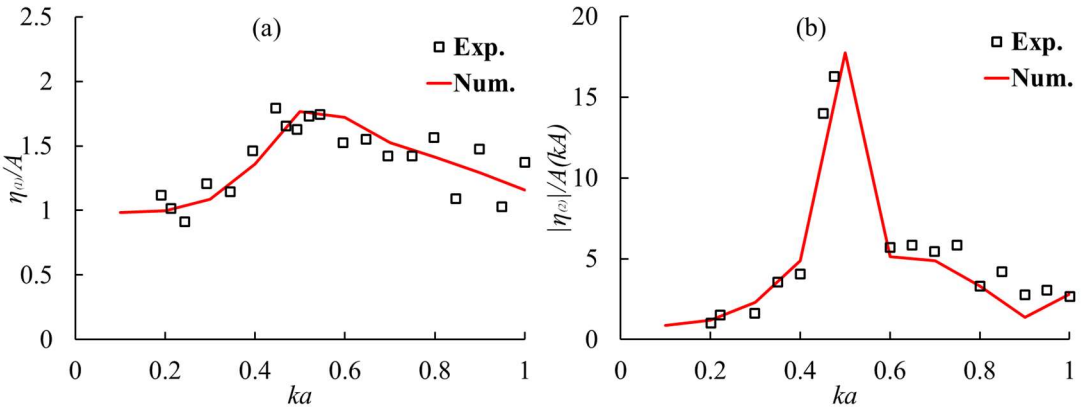

Fig. 7 First-order (a) and second-order (b) non-dimensional amplitudes of the free surface elevation. Numerical result vs. Experimental result (Giorgio et al., 2004) ($\eta_{(1)}$ is the first-order surface elevation component; $\eta_{(2)}$ is the second-order surface elevation component; A is the incident wave amplitude; k is the incident wavenumber)

The first-order and the second-order surface elevation components are shown in Fig. 7 (a) and (b) respectively. The surface elevation monitor point is selected just before the downstream column since this is the peak surface elevation point due to near-trapping phenomenon according to Linton and Evans (1990). In both numerical model and experimental model, the geometric parameter is set a/d=0.275 (a is the radius of the column and d is the distance between two column centres). The incident wave is from 45° to excite the four-column structure with potential near-trapping phenomenon. Fig.7 shows a good agreement between the numerical prediction and experimental measurement. According to Malenica et al. (1999), second-order near-trapping occurs at ka=0.5 which represents the half frequency of the linear trapping frequency making the peak of the second-order component as shown in Fig. 7 (b). It indicates that the potential theory model employed in the present study can predict the second-order near-trapping in multiple columns.

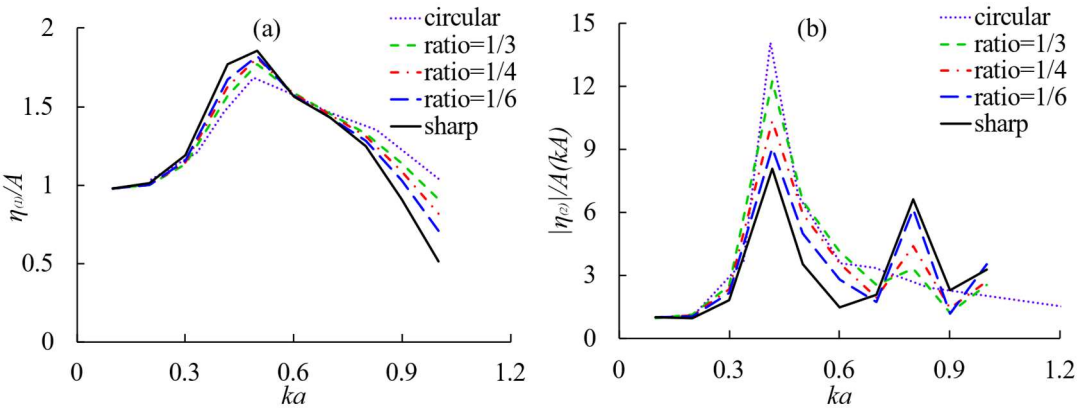

Fig. 8 First-order (a) and second-order (b) non-dimensional amplitudes of the free surface elevation at point#1 (-5.65, 0) in Fig. 9 ($\eta_{(1)}$ is the first-order surface elevation component; $\eta_{(2)}$ is the second-order surface elevation component; A is the incident wave amplitude; k is the incident wavenumber)

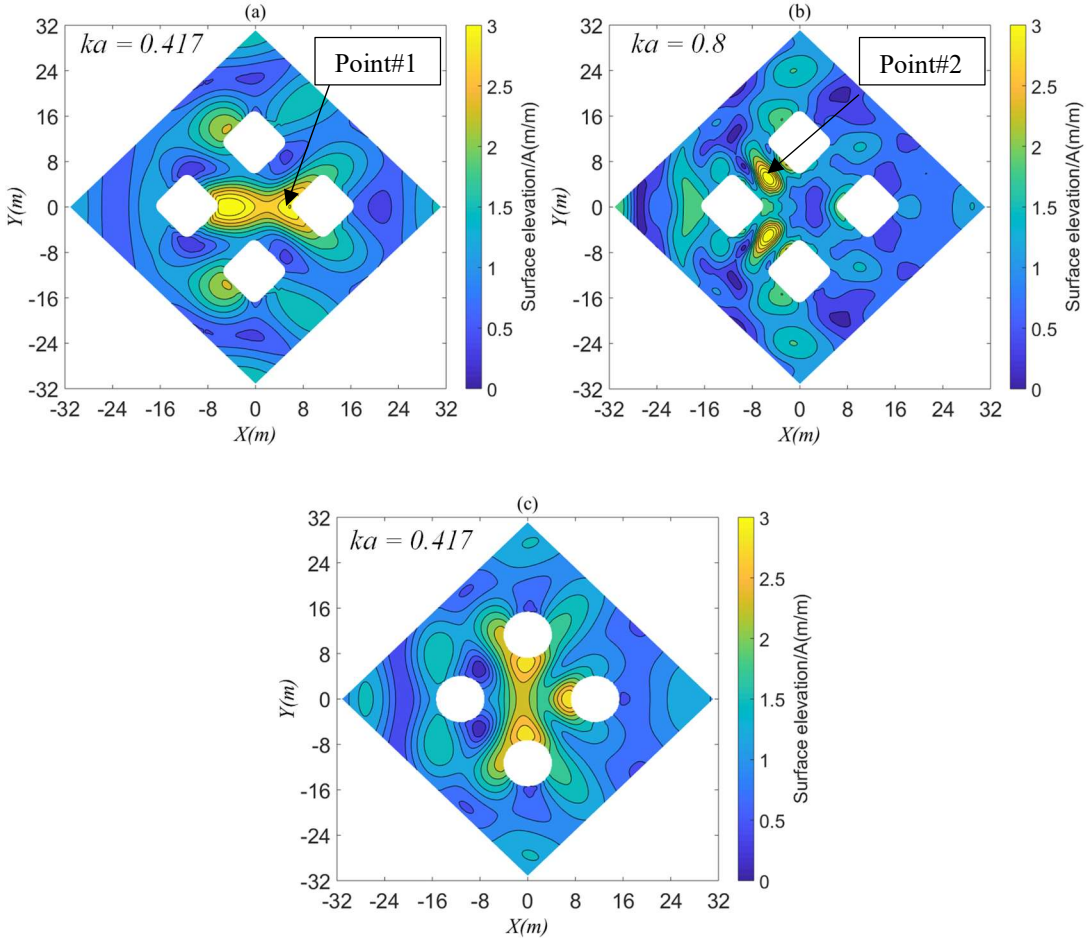

Fig. 9 Surface elevation contour around columns with 45° incident wave (a) rounded-corner square columns (ratio = 1/6) at ka = 0.417; (b) rounded-corner square columns (ratio = 1/6) at ka = 0.8; (c) circular columns at ka = 0.417 and points for surface elevation components analysis point#1 (-5.65, 0) and point#2 (-5.65, 5.65)

Similarly, for rounded-corner square columns, the surface elevation components at point#1 (-5.65, 0) before the downstream rounded-corner squared columns are presented in Fig. 8 to investigate whether the near-trapping mode observed for circular columns are still valid for round square columns. The surface elevation around square and rounded-corner square columns are calculated along the increasing scatter parameter as shown in Fig 8. The rate of the diameter of the column and the distance is set to a/d = 0.25 which is the same as that in Malenica et al. (1999) for circular columns. The first-order surface elevation component (Fig. 8 (a)) around different kinds of columns has a similar trend with increasing scatter parameter. The maximum

first-order surface elevation amplitude increases as the corner ratio changes from circular to sharp. As described by Linton and Evans (1990) and Malenica et al. (1999), the second-order trapping frequency is ka = 0.417 for four circular cylinders with two times of diameter distance from centre to centre. It is shown that the second-order near-trapping occurs at ka = 0.417, thus forming an unusual peak of the second-order surface component in front of the downstream cylinder in Fig. 8 (b). There is an obvious difference between the surface elevation excited by the rounded-corner column and the circular column, that is, the second-order surface elevation component caused by the square and rounded corner square column has two distinct peaks (ka = 0.417 and ka = 0.8), while the cylinder only causes one peak (ka = 0.417). In order to determine whether the two peaks of the second-order surface elevation component cause near-trapping among rounded-corner square columns, the contours of wave surface elevation around the column group are plotted in Fig. 9 (a) and (b) for ka = 0.417 and ka = 0.8 respectively. At the same time, the contour of wave surface elevation around the four circular columns with near-trapping phenomenon at ka = 0.417 is plotted in Fig. 9 (c) for comparison. As shown in Fig. 9, for ka = 0.417 (Fig. 9 (a)), the peak surface elevation is located in the area surrounded by four rounded-corner square columns, which is similar to the surface elevation around the circular columns in Fig. 9 (c). However, for ka = 0.8 (Fig. 9 (b)), there is no peak of surface elevation in the same region surrounded by the rounded corner square columns as observed for ka = 0.417. On the contrary, a pair of peak surface elevations appear in the space between upstream and middle stream columns. It indicates that the peak of the second-order surface elevation component in front of the downstream column at ka = 0.8 is independent of the near-trapping, which is attributed to the superposition of the second-order components of the diffraction by different columns.

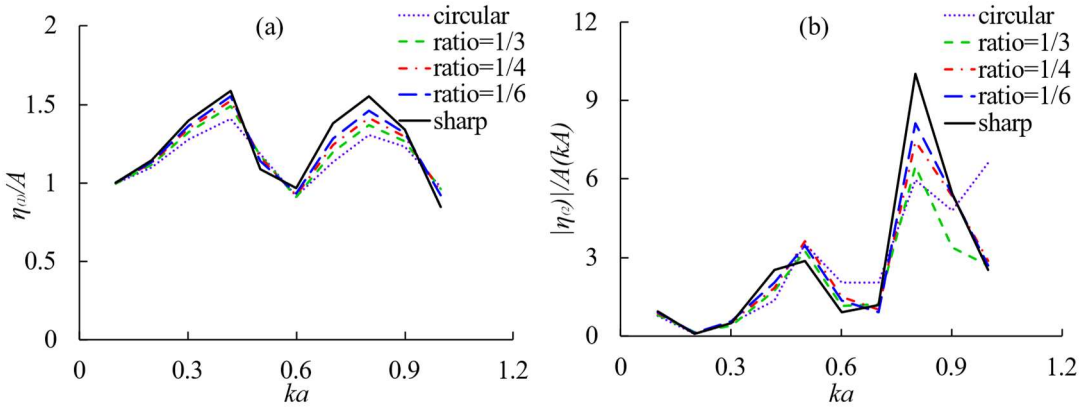

Fig. 10 First-order (a) and second-order (b) non-dimensional amplitudes of the free surface elevation at point #2 (-5.65, 5.65) in Fig. 9 ($\eta_{(1)}$ is the first-order surface elevation component; $\eta_{(2)}$ is the second-order surface elevation component; A is the incident wave amplitude; k is the incident wavenumber)

In Fig 9 (b), it can be easily seen that there is an obvious peak between the upstream column and middle stream column. The analysis of the surface elevation components at point#2 (-5.65, 5.65) which is between these columns is carried out and the results are compared with the surface elevation components excited by circular columns in Fig.10. There are two similar peaks at ka=0.417 and ka=0.8 in the first-order surface elevation component as shown in Fig.10 (a). However, there is no obvious peak at point#2 (-5.65, 5.65) shown in the contour of surface elevation at ka = 0.417 in Fig.9 (a). It indicates that the first-order elevation component of the peaks appearing insufficient to lead to the total peak surface elevation. In other words, the contribution of peak surface elevation seen at ka = 0.8 is the second-order surface elevation component. It is shown that the rounded-corner square column leads to the peak of the second-order surface elevation component (Fig.10 (b)). The sharp corner columns lead to the highest second-order surface elevation component. The peak value of the second-order surface elevation component decreases with the increasing corner ratio. It is noted that the flat part of the square columns makes the wave reflection between columns much stronger than circular columns. This should be taken into consideration in the design of the offshore structures with square columns.

4.2.2 Surface elevation in the multiple columns

Since the square columns have flat panel parts, there is strong wave reflection between two adjacent columns. Therefore, the contour of the surface elevation around the square columns and the detailed surface elevation components are further analyzed. In addition to that the surface elevation between adjacent columns in 45° incident wave discussed in the previous section, the surface elevation around the multiple columns under 0° incident wave examined in this section.

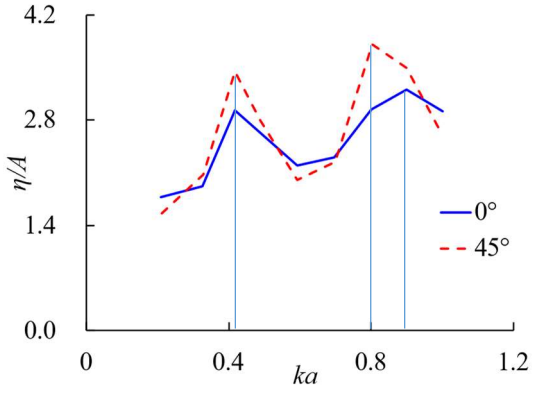

Fig. 11 Maximum surface elevation around four fixed rounded-corner square columns (ratio=1/6) with two times diameter leg space (η is the total surface elevation; A is the incident wave amplitude)

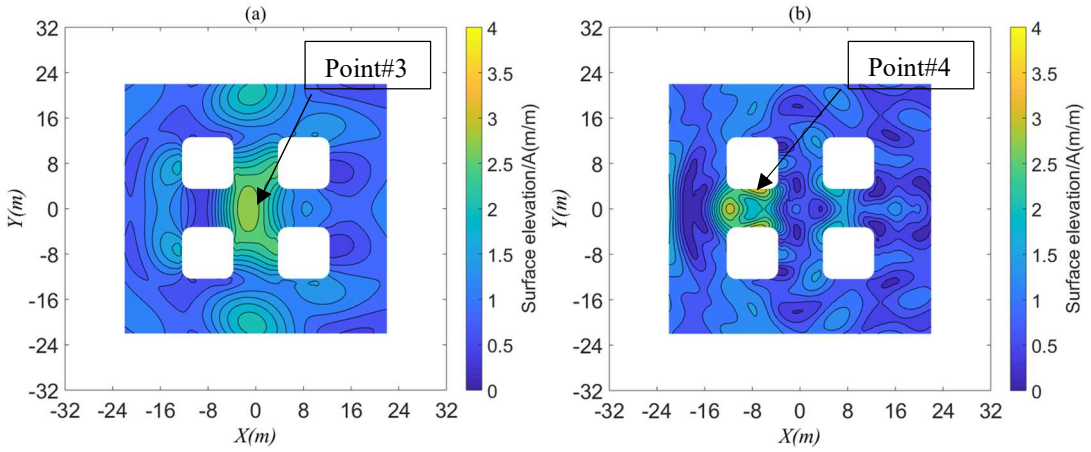

Fig. 12 Contour of surface elevation near rounded-corner square columns (ratio = 1/6) with 0° incident wave (a) *ka* = 0.417; (b) *ka* = 0.9 and points for surface elevation components analysis point#3 (0, 0) and point#4 (-8, 4).

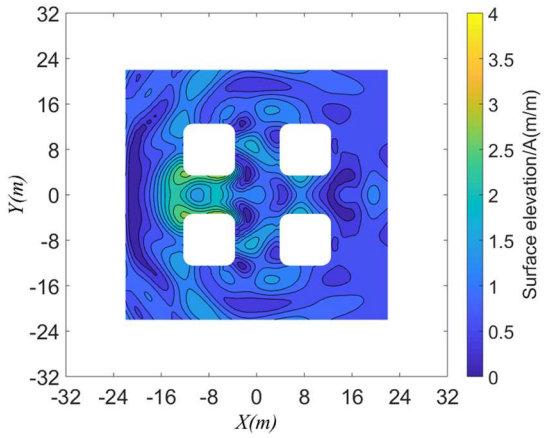

Fig.13 Contour of surface elevation near rounded-corner square columns (ratio = 1/6) with 0° incident wave at *ka* = 0.8;

The maximum surface elevation around four rounded-corner square is shown in Fig 11. It can be seen that there are two peaks for the 0°incident wave at *ka*=0.417 and *ka*=0.9 while there are also two peaks at *ka*=0.417 and *ka*=0.8 under 45°incident wave. The contours of surface elevation around the rounded-corner square columns (ratio=1/6) at *ka*=0.417 and *ka*=0.9 under 0°incident wave are plotted in Fig 12 (a) and (b). It is noted that a single peak surface elevation occurs at the center of the area enclosed by the four rounded-corner square columns nearing the upstream columns at *ka*=0.417. In contrast, two distinct peaks of surface elevation can be clearly seen near the inner boundaries of the two upstream columns at *ka*=0.9. The center of the geometry is selected as point#3 (0, 0) shown in Fig.12(a) to investigate the source of the surface elevation peak when *ka*=0.417. Since the whole configuration is symmetrical, the point

near the inner boundaries of one of the upstream columns is selected as point#4 (-8, 4) shown in Fig.12(b) to investigate the source of the peak surface elevation peak when *ka*=0.9.

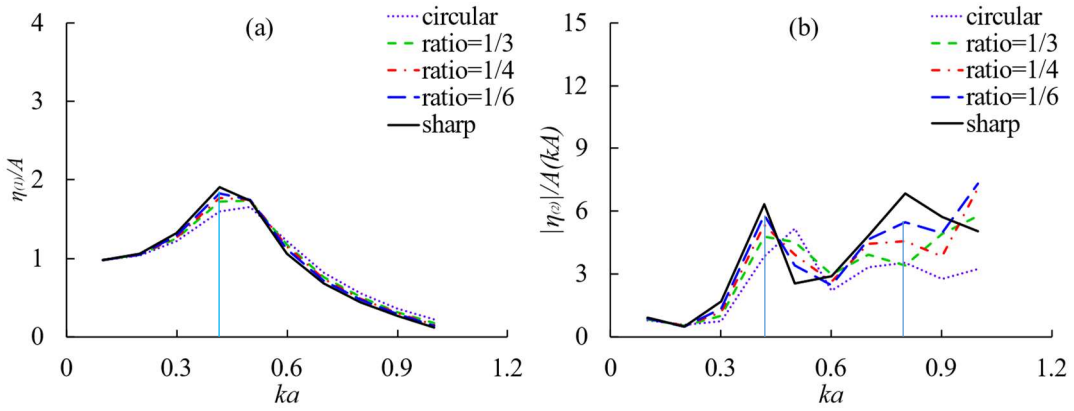

Fig.14 First-order (a) and second-order (b) non-dimensional amplitudes of the free surface elevation at geometric centre point #3 (0, 0) in Fig.12 ($\eta_{(1)}$ is the first-order surface elevation component; $\eta_{(2)}$ is the second-order surface elevation component; A is the incident wave amplitude; k is the incident wavenumber)

The first-order and second-order surface elevation components at geometric center point (0, 0) are shown in Fig 14 (a) and (b) respectively. There is one peak of first-order surface elevation at *ka*=0.417 shown in Fig 14 (a) while two peaks of the second-order surface elevation are clearly observed at *ka*=0.417 and *ka*=0.8 respectively as shown in Fig 14 (b). There is no peak surface elevation at the geometric center point at *ka*=0.8 as shown in Fig 13 indicating that the peak of the second-order component shown in Fig 14 (b) has little contribution to the total surface elevation amplitude. It indicates that the peak of surface elevation at *ka*=0.417 is dominated by the first-order surface elevation component. It can be further demonstrated by the ratio between the second-order and the first-order surface elevation at the geometric centre point which equals 3/5 when *ka*=0.417. The first-order surface elevation component increases gradually with *ka* until reaching its peak at *ka*=0.417 rather than a sudden jump, which means that the peak of the first-order surface elevation is not caused by resonance phenomenon between columns. It indicates that the peak at the geometric center point is primarily caused by the superposition of the incident waves and diffraction waves inside the four columns.

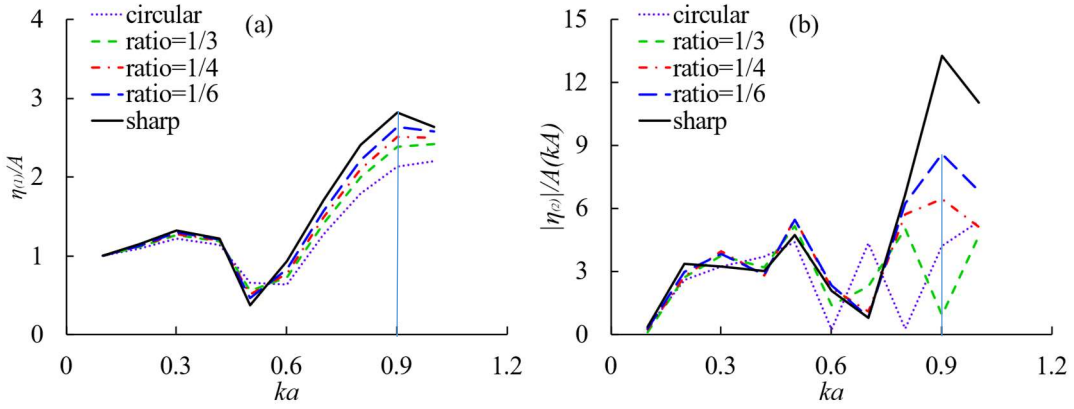

Fig.15 First-order (a) and second-order (b) non-dimensional amplitudes of the free surface elevation at point #4 (-8, 4) in Fig. 12 ($\eta_{(1)}$ is the first-order surface elevation component; $\eta_{(2)}$ is the second-order surface elevation component; A is the incident wave amplitude; k is the incident wavenumber)

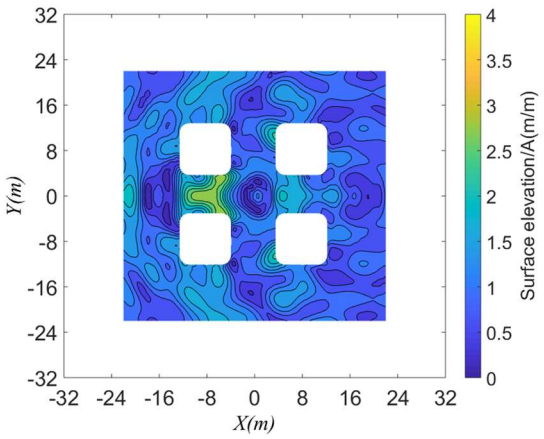

Fig.16 Contour of surface elevation near rounded-corner square columns (ratio = 1/6) with 0° incident wave at ka = 1.0;

In Fig.15, the surface elevation components at the point near the upstream columns (point #4) are analyzed in first-order (Fig. 15(a)) and second-order (Fig. 15(b)). For rounded-corner ratio 1/6, the highest first-order surface elevation component occurs at ka=0.9 in Fig 15 (a). There is also a significant peak of the second-order surface elevation component at ka=0.9 as shown in Fig 15 (b). The first-order surface component at point#4 changes little from ka=0.9 to ka=1.0. However, there is a large reduction of second-order surface elevation component with increasing ka from 0.9 to 1.0 shown in Fig 15 (b). The different trend of the first- and second-order of the surface elevation components at point#4 is applied to investigate the source of the peak surface elevation at ka=0.9. The contour of the surface elevation around rounded-corner square columns at ka=1.0 is also plotted in Fig 16 as a comparison since the different contributions of first-order and second-order surface elevation components from ka=0.9 to 1.0.

In Fig16, the peak of total surface elevation occurs in the middle of the upstream columns rather than the position near columns. Comparing the surface elevation contour at ka=0.9 (Fig12 (b)) and ka=1.0 (Fig16), it is noted that the surface elevation amplitude at point#4 reduces significantly with increasing ka=0.9 to ka=1.0.

It indicates that the first-order component does not have a decisive influence on the peak of surface elevation at point#4, but the second-order component causes the peak at ka = 0.9. Since the second-order component peak does not occur suddenly but gradually climbs (not generated in a narrow frequency band), the peak of the second-order surface component is just caused by the superposition of waves. In addition, the peak of the second-order surface component is decreasing with higher ratio of corner of column. The impact of the ratio on the second-order component is more significant than that on the first-order component. It can be explained that with the lower ratio of corner, there is a larger parallel part of columns which would lead to stronger reflection of waves. The strong reflection wave makes the higher surface elevation and stronger nonlinearity.

5. Conclusions

The wave run-up along the columns and surface elevation around the multiple columns are investigated in the present study. For the incident wave $Kc=A/a<\mathcal{O}(1)$ and wave steepness H/L<0.14, the potential theory is applied to the calculation of wave run-up along columns and surface elevation. The wave run-up and peak surface elevation caused by wave interaction with rounded-corner square columns with different corner ratios are investigated and compared with the existing results of circular columns. The following conclusions can be drawn:

- The increasing ratio of corner radius results in a lower wave run-up along the rounded-corner square column under 0° incident wave, and a higher wave run-up under 45° incident wave.
- Two mechanisms are clearly identified being responsible to the peak surface elevation namely superposition and near-trapping for wave interaction with multiple columns of both circular and rounded-corner square cross-sectional shape.
- Near-trapping frequency model for multiple circular columns is demonstrated still effective for the four rounded-corner square columns. However, the peak surface elevation due to near-trapping reduces with the sharper corner. The square columns with carefully designed rounded-corner can be applied in the offshore structures with multi-column to avoid the peak surface elevation caused by near-trapping.

- Quantitative demonstration revealed that the impact of the column's corner ratio on the second-order component is significantly larger than that on the first-order component. The peak of the second-order surface elevation component decreases with higher corner ratio of column.

- During wave interaction with four rounded-corner square columns, a single peak surface elevation under 0° incident wave is attributed to superposition, while different peaks of surface elevation depending on scatting parameter under 45° incident wave are demonstrated due to near-trapping and superposition, respectively.

References

Abdussamie, N., Drobyshevski, Y., Ojeda, R., Thomas, G., Amin, W., 2017. Experimental investigation of wave-in-deck impact events on a TLP model. Ocean Engineering 142, 541-562.

Chakrabarti, S.K., 1978. Wave forces on multiple vertical cylinders. Journal of the waterway, port, coastal and ocean division 104 (2), 147-161.

Chen, L., Zang, J., Hillis, A., Morgan, G., Plummer, A., 2014. Numerical investigation of wave–structure interaction using OpenFOAM. Ocean Engineering 88, 91-109.

Contento, G., D'este, F., Sicchiero, M., Codiglia, R., Calza, M., 2004. Run-up and wave forces on an array of vertical circular cylinders: Experimental study on the second order near trapping, The Fourteenth International Offshore and Polar Engineering Conference. International Society of Offshore and Polar Engineers.

Dong, Z., Zhan, J.-m., 2009. Numerical Modeling of Wave Evolution and Run-up in Shallow Water. Journal of Hydrodynamics 21 (6), 731-738.

Evans, D., Porter, R., 1997. Near-trapping of waves by circular arrays of vertical cylinders. Applied Ocean Research 19 (2), 83-99.

Fang, Z., Xiao, L., Guo, Y., Kou, Y., Li, J., 2018. Wave run-up on a fixed surface-piercing square column using multi-layer barrier. Applied Ocean Research 71, 105-118.

Grice, J., Taylor, P., Taylor, R.E., 2013. Near-trapping effects for multi-column structures in deterministic and random waves. Ocean Engineering 58, 60-77.

Kagemoto, H., Murai, M., Fujii, T., 2014. Second-order resonance among an array of two rows of vertical circular cylinders. Applied Ocean Research 47, 192-198.

546 Kim, M.-H., Yue, D.K., 1989. The complete second-order diffraction solution for an
547 axisymmetric body Part 1. Monochromatic incident waves. Journal of Fluid Mechanics 200,
548 235-264.

549 Kim, M.-H., Yue, D.K., 1990. The complete second-order diffraction solution for an
550 axisymmetric body Part 2. Bichromatic incident waves and body motions. Journal of Fluid
551 Mechanics 211, 557-593.

552 Kriebel, D.L., 1992. Nonlinear wave interaction with a vertical circular cylinder. Part II: Wave
553 run-up. Ocean Engineering 19 (1), 75-99.

554 Kristiansen, T., Baarholm, R., Stansberg, C.T., 2004. Validation of second-order analysis in
555 predicting diffracted wave elevation around a vertical circular cylinder, The Fourteenth
556 International Offshore and Polar Engineering Conference. International Society of Offshore
557 and Polar Engineers.

558 Lee, C.-H., 1995. WAMIT THEORY MANUAL.

559 Lin, Y.-H., Chen, J.-F., Lu, P.-Y., 2017. A CFD model for simulating wave run-ups and wave
560 loads in case of different wind turbine foundations influenced by nonlinear waves. Ocean
561 Engineering 129, 428-440.

562 Linton, C., Evans, D., 1990. The interaction of waves with arrays of vertical circular cylinders.
563 Journal of Fluid Mechanics 215, 549-569.

564 Low, Y., 2010. Influence of the setdown of a tension leg platform on the extreme air-gap
565 response. Applied Ocean Research 32 (1), 11-19.

566 Lu, W., Li, X., Zhang, X., Tian, X., Guo, X., 2020. Experimental study on the wave run-up and
567 air-gap response of a three-column semi-submersible platform. Ocean Engineering 203, 107-
568 253.

569 Lu, W., Yang, J., Xiao, L., Guo, X., Li, X., 2020. Experimental investigation of wave run-up
570 and air-gap responses. Ocean Engineering 202, 107-116.

571 Malenica, Š., Taylor, R.E., Huang, J., 1999. Second-order water wave diffraction by an array
572 of vertical cylinders. Journal of Fluid Mechanics 390.

573 Morris-Thomas, M., Thiagarajan, K., 2004. The run-up on a cylinder in progressive surface
574 gravity waves: harmonic components. Applied Ocean Research 26 (3-4), 98-113.

575 Niedzwecki, J., Huston, J., 1992. Wave interaction with tension leg platforms. Ocean
576 Engineering 19 (1), 21-37.

577 Raman, H., Shankar, N.J., Venkatanarasaiah, P., 1977. Nonlinear wave interaction with vertical
578 cylinder of large diameter. Journal of Ship Research 21 (02), 120-124.

579 Raman, H., Venkatanarasaiah, P., 1976. Forces due to nonlinear waves on vertical cylinders.
580 Journal of the Waterways, Harbors and Coastal Engineering Division 102 (3), 301-316.

581 Shan, T.-b., Yang, J.-m., Li, X., Xiao, L.-f., 2011. Experimental investigation on wave run-up
582 characteristics along columns and air gap response of semi-submersible platform. Journal of
583 Hydrodynamics 23 (5), 625-636.

584 Simos, A.N., Sparano, J.V., Aranha, J.A., Matos, V.L., 2008. 2nd order hydrodynamic effects
585 on resonant heave, pitch and roll motions of a large-volume semi-submersible platform, ASME
586 2008 27th International Conference on Offshore Mechanics and Arctic Engineering. American
587 Society of Mechanical Engineers, pp. 229-237.

588 Sweetman, B., Winterstein, S.R., Meling, T.S., Birknes, J., 2001. Airgap Prediction" Use of
589 Second-Order Diffraction and Multi-Column Models, The Eleventh International Offshore and
590 Polar Engineering Conference. International Society of Offshore and Polar Engineers.

591 Taylor, R.E., Sincock, P., 1989. Wave upwelling effects in TLP and semi-submersible
592 structures. Ocean Engineering 16 (3), 281-306.

593 Wang, C., Wu, G., 2007. Time domain analysis of second-order wave diffraction by an array
594 of vertical cylinders. Journal of Fluids and Structures 23 (4), 605-631.

595 Wang, C., Wu, G., 2010. Interactions between fully nonlinear water waves and cylinder arrays
596 in a wave tank. Ocean Engineering 37 (4), 400-417.

597 Wang, Y., You, Y.-x., 2009. Numerical simulation of interaction of viscous wave fields with a
598 semi-submersible platform [J]. Journal of Hydrodynamics (Ser. A) 6, 018.

599 Xiong, H., Yang, J., Tian, X., 2015. An experimental study on the inline wave force on a
600 truncated vertical cylinder. Ships and Offshore Structures, 1-16.

601
602